AGU PUBLICATIONS

JGR

Journal of Geophysical Research: Space Physics

RESEARCH ARTICLE
10.1002/2016JA023457

Special Section:
Inner Magnetosphere Coupling: Recent Advances

On the variation in the ionospheric response to geomagnetic storms with time of onset

K. R. Greer[1], T. Immel[1], and A. Ridley[2]

[1]Space Sciences Laboratory, University of California, Berkeley, California, USA, [2]Department of Aerospace Engineering, University of Michigan, Ann Arbor, Michigan, USA

Key Points:
- Simulations reproduce observed dependence of ionospheric response to UT of storm onset
- Changes in upper atmospheric neutral winds or composition cannot account for the ionospheric effect at low latitudes
- The implicated driver is the coupling of storm time *F* region winds and Earth's asymmetric magnetic topology

Correspondence to:
K. R. Greer,
katelynn.greer@lasp.colorado.edu

Citation:
Greer, K. R., T. Immel, and A. Ridley (2017), On the variation in the ionospheric response to geomagnetic storms with time of onset, *J. Geophys. Res. Space Physics*, *122*, 4512–4525, doi:10.1002/2016JA023457.

Received 13 SEP 2016
Accepted 15 MAR 2017
Accepted article online 22 MAR 2017
Published online 12 APR 2017

Abstract Recent observations from Immel and Mannucci (2013) have indicated that geomagnetic storms cause larger enhancements in the ionospheric plasma density and total electron content (TEC) in the American sector than anywhere else on the planet. This suggests that the presence of a UT storm onset effect is important for correctly understanding the impact, longitudinal structure, and timing of geomagnetic storms. Using the Global Ionosphere-Thermosphere Model (GITM), we conduct a modeling experiment of the August 2011 geomagnetic storm by modifying the storm arrival time (UT) in Earth's daily rotation and examining the subsequent system response. We find that the simulations reflect the recent studies indicating that the strongest enhancements of TEC are in the American and Pacific longitude sectors of storms with onsets between 1600 UT and 2400 UT. The underlying mechanisms of the strong TEC increases during storm times in these longitude sectors are also examined. Some of the resulting TEC structures may be explained by changes in the $[O]/[N_2]$ ratio (especially in the high latitudes), but it is unable to explain all of the variability in the equatorial regions. Storm time neutral winds and vertical ion motions coupled to Earth's asymmetrical geomagnetic topology appear to be driving the longitude sector variability due to UT storm onset times.

1. Introduction

Interest in understanding the detailed behavior of Earth's ionosphere has increased as reliance on satellite communication and navigation has grown. These technologies are susceptible to unpredicted variability in ionospheric plasma density and intensified density gradients. The availability of these technologies is therefore influenced by ionospheric "weather," and the prediction of ionospheric conditions continues to be challenging because of limitations in the observations of key parameters and numerical models [*Komjathy et al.*, 2005]. Progress in modeling the key influences and drivers of this complex and dynamic region continues to be made. However, with the continued deployment of ground-based line of sight total electron content (TEC) receivers [*Jakowski et al.*, 2002a; *Kintner and Ledvina*, 2005; *Valladares and Chau*, 2012] and space-based occultation receivers [*Jakowski et al.*, 2002b; *Lei et al.*, 2007; *Hajj and Romans*, 1998], there is a growing accurate record of ionospheric plasma. Though spatial and temporal gaps do exist in these records, we are able to observe the global morphology of ionospheric storms in increasing detail. The technologies and systems that are adversely affected by elevated density and sharp density gradients also serve to provide measurements of the changing plasma parameters. These kinds of observations have led to several breakthroughs in our knowledge of the Earth-Sun system behavior during magnetic storms.

The positive ionospheric storm has long been observed in daytime plasma densities, particularly in the afternoon sector [*Mendillo et al.*, 1970; *Burns et al.*, 1995a]. Related inner magnetospheric signatures of ionospheric plasma enhancements were first described by *Grebowsky et al.* [1978] [see *Carpenter et al.*, 1992] and seen in imaging of the plasmasphere by the NASA Imager for Magnetopause-to-Aurora Global Exploration (IMAGE) mission [*Sandel et al.*, 2001; *Burch*, 2003]. Through multipoint measurements of plasma density, it has been shown that plasma density enhancements in the daytime are highly structured and reflect, in part, the development of inner-magnetospheric electric fields that are only manifested during these disturbed periods [*Foster and Rich*, 1998; *Huang et al.*, 2005]. The structure and evolution of ionospheric density enhancements, particularly those observed early in geomagnetic storms, reflect both causes and signatures that extend throughout the geospace system.

Numerical and observational studies of the variability of ionospheric features in the middle and low latitudes have been conducted over the years; however, there are limited studies focused exclusively on longitudinal variability due to the univeral time (UT) onset time in the low latitudes. Explorations of the longitude sector differences of equatorial spread *F* have been conducted by several groups[*Aarons*, 1991; *Fejer et al.*, 1999; *Abdu et al.*, 2005; *Oladipo et al.*, 2014], and several studies have found an impact of longitudinal effects on the equatorial electroject (EEJ) [*England et al.*, 2006; *Klimenko and Klimenko*, 2015; *Yizengaw et al.*, 2014; *Phani Chandrasekhar et al.*, 2014]. It has also been recognized that the neutral atmosphere plays a critical role through nonmigrating tidal influences [*Immel et al.*, 2006; *Forbes et al.*, 2008; *Maute et al.*, 2015] and longitudinally dependent thermospheric winds [*Fuller-Rowell et al.*, 1994; *Sojka et al.*, 2012] in the distribution of plasma. And while there are numerous studies examining enhancements of TEC [*Ho et al.*, 1996; *Kelley et al.*, 2004; *Mendillo*, 2006] (a proxy measurement for plasma density) during geomagnetic storms, far fewer studies have been concerned with the variability of that TEC distribution based on the UT time (longitudinally dependent) onset of storms at low and middle latitudes [*Immel and Mannucci*, 2013; *Coster et al.*, 2007]. *Mendillo* [2006] conducted a statistical epoch analysis of TEC storms observed by Air Force Cambridge Research Laboratories (AFCRL) locations in the Northern Hemisphere organized by local time (LT), but the actual UT onset time was not kept as a factor and the lowest latitude site was Kennedy Space Flight Center. An idealized modeling study conducted by *Sojka et al.* [2012] found that TEC enhancements had preferential longitudinal sectors in the midlatitudes based on onset times, but limitations of the model meant that low-latitude and equatorial processes were explicitly excluded from their analysis. Through a statistical examination of ionospheric conditions during all geomagnetic storms observed during the 1998–2007 epoch, *Immel and Mannucci* [2013] found that for storms with onsets between 1800 UT and 2200 UT, large storm time increases in daytime ionospheric plasma content exists in the American sector and is stronger there than in any other sector. However, the methodology of this study was limited by being obliged to draw conclusions from sparse data (TEC observations are especially scarce over oceans) and comparisons of phenomenologically disparate geomagnetic storms. Additionally, their examination of observational TEC maps is not able to isolate and implicate the driving mechanisms responsible for this UT onset longitudinal variability; coupled global numerical simulations would be ideal for examining this through numerical experiments of storms that develop at different times but are otherwise identical storms. It has yet to be shown that available coupled models have been able to replicate the zonal effect observed by *Immel and Mannucci* [2013] or reproduce a UT variation in storm densities at the middle and low latitudes as observed in the JPL GNSS-TEC (Jet Propulsion Laboratory's Global Navigation Satellite System) data assimilated from quiet and storm time measurements. The use of sophisticated coupled numerical simulations allows us to investigate whether the observed UT onset longitudinal sector variability is a physically driven phenomenon or potentially due to observational geometry or sparseness of data over particular geographic regions. Reproducing this phenomenon and investigating its drivers comprise the motivations of this work.

This study investigates a case in August 2011 where a solar wind disturbance impacted geospace and drove an isolated but strong geomagnetic storm response. We use the specific inputs of this storm to investigate the importance of the UT storm onset and longitudinal sector response. Here we show that the coupled Global Ionosphere-Thermosphere Model (GITM), using time-shifted magnetospheric inputs developed using BATS-R-US (Block Adaptive Tree SolarWind-Roe Upwind Scheme), displays a remarkable low- and middle-latitude asymmetry in responses to the storm. Further, it indicates for the first time that chemical, dynamical, and electrodynamic drivers all have the potential to play a key role in supporting the larger TEC increases observed in the South American sector during this August 2011 storm. We specifically compare the wind dynamo, magnetospheric potentials, and thermospheric composition to the storm-enhanced density to identify the key drivers of the plasma density increases for different storm onset UT.

2. Model

A coupled model of the ionosphere and thermosphere that simultaneously captures the physics of both the neutral and plasma environments is required for this investigation. This is because the variable composition and dynamics of the upper atmosphere during geomagnetic storms are critical for modifying the ionosphere and impacting TEC variability. By repeatedly modeling the same single observed storm, we remove the inherent variability that is present in the comparisons of different historical storms having different UT onset times and perhaps wildly different solar wind conditions, seasons, durations, and strengths (such as was done by *Immel and Mannucci* [2013]). Further, using a coupled model may allow the probing of individual

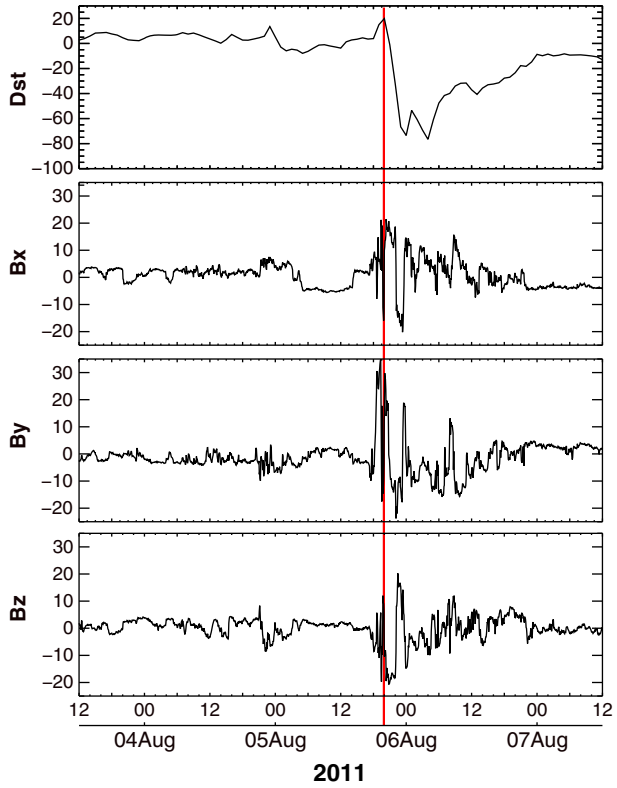

Figure 1. August 2011 storm *Dst* index and observed IMF properties.

driving forces that influence the longitudinal sector variability due to UT onset.

The model used in this study is the Global Ionosphere-Thermosphere Model (GITM) developed at the University of Michigan by *Ridley et al.* [2006]. GITM is a three-dimensional, spherical coordinate model that nonhydrostatically solves the continuity, momentum, and energy equations of the thermosphere and ionosphere using realistic source terms. Ion flow velocities are assumed to be steady state and solved from the momentum equations. Physical drivers of the model include auroral particle precipitation, solar extreme ultraviolet (EUV) flux, and tides which are determined from the empirical Mass Spectrometer Incoherent Scatter (MSIS-86) model for the neutral atmosphere below 100 km [*Hedin*, 1987]. The vertical coordinate is altitude, while the International Geomagnetic Reference Field (IGRF) is used for the magnetic topology. The equatorial electrodynamics are self-consistently solved [*Richmond*, 1995]. The high-latitude electric fields are supplied by the Space Weather Modeling Framework (SWMF) at the Goddard Space Flight Center's Community Coordinated Modeling Center (CCMC). The CCMC archives these inputs, and they may be accessed by the public on their website or by request.

For the experimental runs, the geographical grid was specified as 5° longitude × 2° latitude with an altitude range of 100 km to 600 km. A value of 1750 was used for the eddy diffusion coefficient [*Pawlowski and Ridley*, 2009]. The model was allowed 48 simulation hours to spin-up using Weimer high-latitude electric fields [*Weimer*, 1996], then, 15 h before the onset of storm conditions (and throughout the duration of the storm), the model was driven by the more realistic high-latitude electric field drivers provided by the Space Weather Modeling Framework's BATS-R-US model (please visit SWMF at http://ccmc.gsfc.nasa.gov/ for more information) [*Tóth et al.*, 2005].

A limitation of GITM may sometimes be seen in unusual nighttime modeled plasma values that do not accurately reflect observed plasma densities, particularly at midlatitudes. Factors in the current version of GITM that may be contributing to this are that vertical advection of ions is computed using $\ln(\rho)$ as the quantity in the solver for the vertical advection scheme (to linearize the exponentially decreasing mass density with altitude) and a model simplification introduced to the continuity equation for the ions which assumes that the contribution from the divergence of the wind field is negligible. Further investigation of this model during quiet time conditions is discussed in *Vichare et al.* [2012]. Given that this study is focused on differences between model runs under identical inputs shifted in UT, for our conclusions these limitations are of little consequence.

3. Methods

To investigate UT-dependent responses of the ionosphere, we used the moderately strong geomagnetic storm that was observed in August 2011 during the International Union of Radio Science (URSI) World Day Campaign. The sun during solar cycle 24 has been unusually quiet, but 2011 was part of the two-peaked solar maximum when there were more frequent flares and coronal mass ejections (CMEs). The *Dst* (nT) and interplanetary magnetic field (IMF) for 04:00 UT on 5 August through 12:00 UT on 7 August 2011 are shown in Figure 1. The intensity of the IMF was measured by the Advanced Composition Explorer (ACE), while the *Dst*

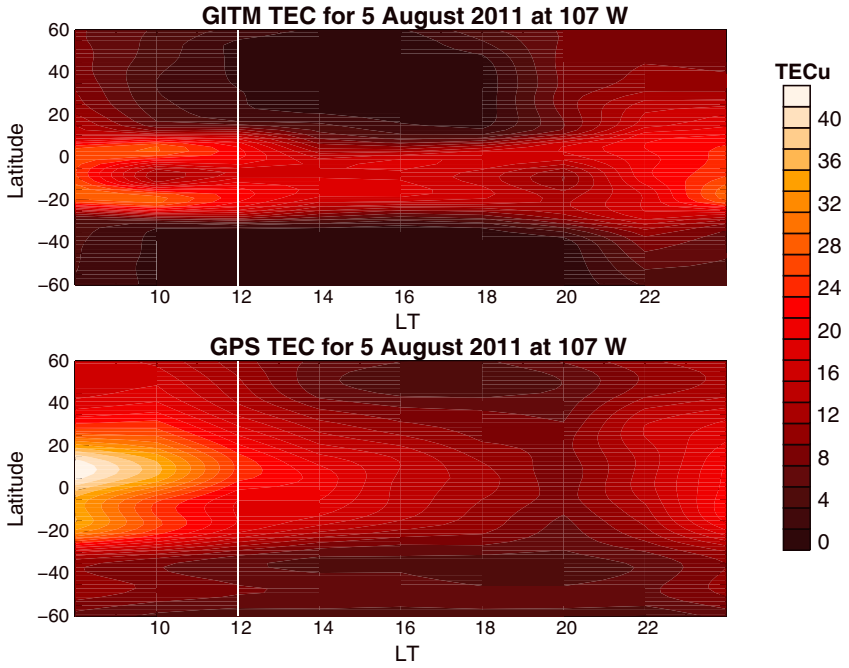

Figure 2. August 2011 storm TEC (in TECU) at 107°W longitude as observed by (bottom) GPS and (top) GITM. TEC is illustrated in local time (LT) and latitude at a constant longitude. The white vertical line at local 12 noon indicates the onset of the geomagnetic storm (5 August 2011 19:06 UT).

is provided by the Kyoto World Data Center [*Sugiura*, 1964]. Two CMEs were propelled from the Sun, merged, and arrived at Earth, causing an abrupt increase in the dynamic pressure, strong oscillations in all components of the IMF [*Huang et al.*, 2014], and a brief rise in *Dst* followed by a precipitous drop. The vertical red line in Figure 1 indicates the onset time of the storm at 19:06 UT on 5 August 2011. The *Dst* index reached a minimum value of −115 nT at 04:00 UT on 6 August 2011, while the *Kp* index reached 7+, indicative of a strong geomagnetic storm. An extended recovery followed.

Although GITM has been extensively validated in literature [*Ridley et al.*, 2006; *Deng et al.*, 2008; *Pawlowski et al.*, 2008; *Zhu and Ridley*, 2016; *Zhu et al.*, 2016], Figure 2 shows a comparison of TEC obtained from GNSS (GPS) and modeled by GITM for the geomagnetic storm shown in Figure 1. GPS TEC data were obtained from ftp://spdf.gsfc.nasa.gov/pub/data/gps/ and are 2-hourly maps of TEC as derived by the International GNSS Service (IGS)[*Kouba*, 2009]. Figure 2 shows the progression of the TEC in local time (LT) in the equatorial and midlatitudes at 107°W (North America and eastern Pacific sector) in TECU (total electron content unit, 10^{16} e^{-} m^{-2}). The white vertical line at local 12 noon indicates the onset of the geomagnetic storm (5 August 2011 19:06 UT). In general, GITM captures the timing of the evolving structure well but tends to underestimate the afternoon midlatitude TEC. Given the modeling simplifications made by GITM, it appears that at low latitudes the vertical gradient in the ion velocity in the vertical direction may be significant and strongly affect the plasma density structure with height, causing the ion densities to be lofted too high in the ionosphere late in the day, reducing the loss rates, and causing the densities at night to be too large. Nonetheless, the plasma densities and associated TEC results from GITM during the daytime are reliable and appropriate for use in studies of *relative* change in TEC such as this particular study.

Using GITM, we modeled this storm with the observed timing, where at 19:06 UT the sector around 107°W was at solar local noon. For subsequent runs the arrival time of the driving solar wind inputs were shifted in time to examine how the ionosphere responded to different UT storm onsets, for the same solar wind conditions. The storm onset times were shifted by −12, −9, −6, −3, +3, +6, +9, and +12 h, which correspond to sunward arrival sectors (1200 LT) of 72°E, 27°E, 17°W, 62°W, 152°W, 162°E, 117°E, and 72°E, respectively.

To obtain a picture of how ionospheric conditions vary with UT timing of the storm, we make use of global maps of total electron content (TEC). These are calculated from column plasma densities produced by GITM. To evaluate changes in the ionosphere produced by storms, the change between quiet solar wind conditions

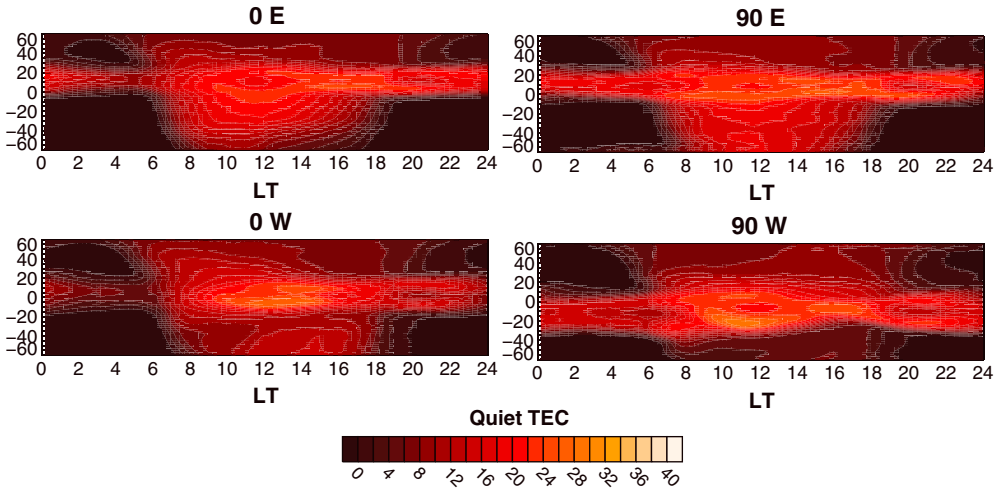

Figure 3. Quiet TEC as modeled by GITM for constant longitude sectors in local time and latitude.

to storm conditions can be compared at any longitude sector or local time. The mean quiet time TEC as modeled by GITM is shown in Figure 3 for the longitude sectors of 0°E, 90°E, 0°W, and 90°W. This mean quiet time was determined by using the 15 h prior to storm onset for all nine model runs (since these runs were shifted in time by up to 12 h, it allowed for the buildup of 24 h of quiet ionosphere). The quiet TEC was calculated for each longitude-latitude grid point, every 900 s (15 minutes). In each case, the equatorial ionospheric anomaly (EIA) is prominent at low latitudes from approximately 1000 LT to 1800 LT at all longitudes. Maximum quiet-condition TEC values generally reached approximately 35 TECU in the southern crest of the EIA. Even during quiet ionospheric conditions, Figure 3 clearly shows that different longitude sectors have different local time responses in terms of magnitude, timing, and structure of plasma in the ionosphere. It is critical to take into account this natural quiet time variability when evaluating the ionosphere's response to the storm conditions.

4. TEC Plasma Results

The difference between active and quiet conditions for each of the experimental storm onset times is shown in Figure 4. Each panel is for a constant longitude focusing on the afternoon and evening hours; the colors indicate the absolute difference, $TEC_{Storm} - TEC_{Quiet}$, in latitude and local time. The longitude displayed corresponds to the longitude of 1200 LT (the sunward sector) at the time of the onset of the storm, and a stereographic map of the Earth is provided for geographic reference. These experiments span ±12 h from the observed onset at 1900 UT. Additionally, these results are also presented as percent change in TEC for additional insight in Figure 5.

All the experiments share some general features. At low latitudes there is deepening of the depletion of plasma in the trough of the EIA, especially pronounced after 1800 LT. On either side of this depletion, there is an augmentation of TEC. This is consistent with the observations from *Immel and Mannucci* [2013] of historical storm TEC with *Dst* indices of < -100 nT where there is an enhancement of the fountain effect driven by penetration of magnetospheric electric fields into the low latitudes [*Mannucci et al.*, 2005].

However, Figure 4 also exhibits TEC structures that are slowly varying between the different storm onset experiments. In the evening hours, the sectors between 62°W and 162°E (the Americas and central Pacific) display an intense but narrow tongue of concentrated TEC in the Southern Hemisphere just below the equatorial trough, an increase of approximately 20 TECU or percent change of nearly 90%. Hemispheric asymmetry is likely due to the season and configuration of the geomagnetic field. Large positive differences extend to higher latitudes between noon and 1400 LT in the sectors between 152°W and 117°E, over the Pacific ocean and eastern Asia, of 10–12 TECU or a percent change of 40–60%. The western Pacific sector around 162°E is the only sector that experiences a period (around 1715 LT) where the trough feature in the EIA is diminished.

It is evident from these results that the American and Pacific sectors in the Southern Hemisphere experience the strongest TEC enhancements, in intensity, duration, and latitudinal extent for these storm conditions.

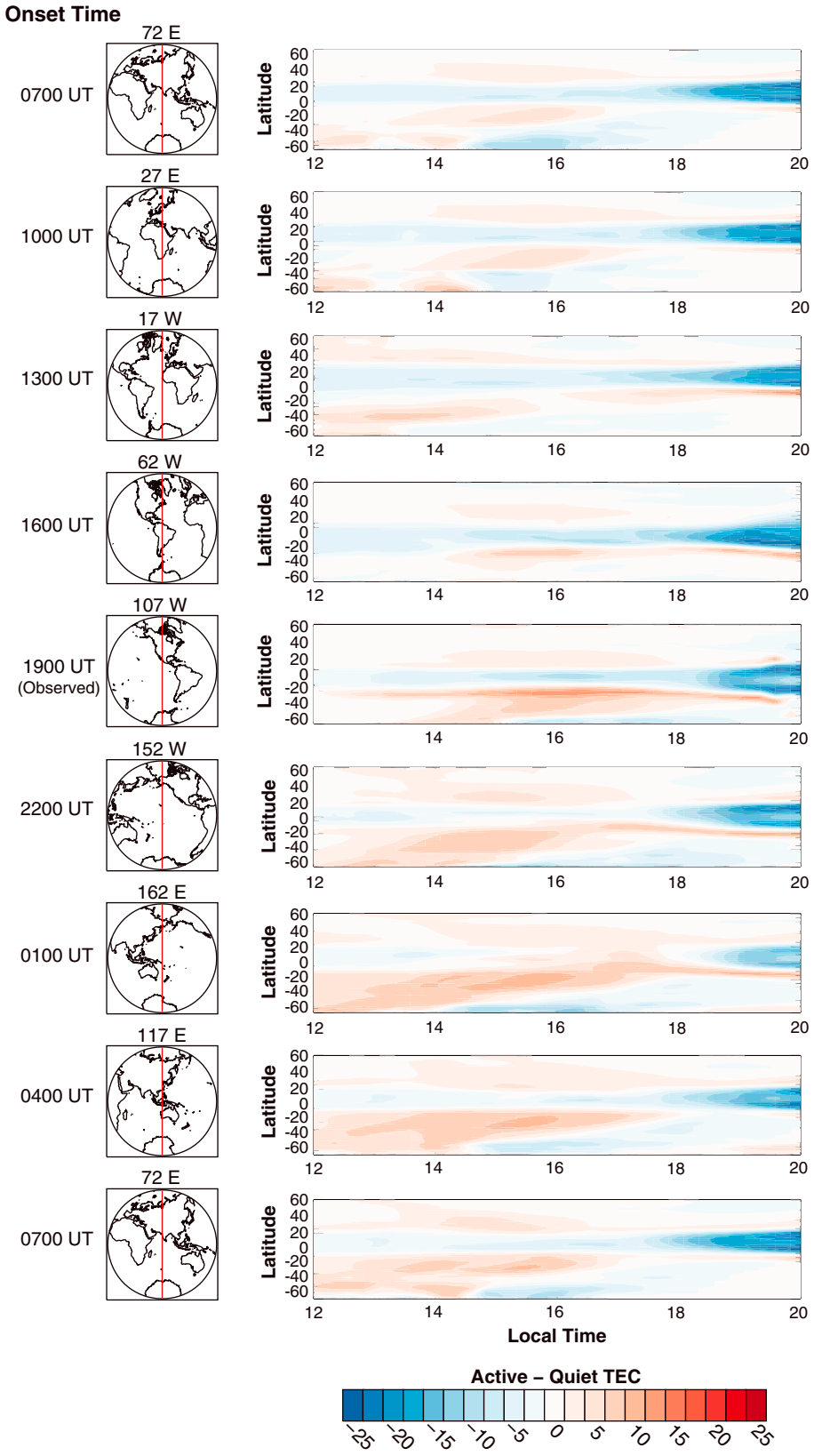

Figure 4. Difference between quiet TEC and storm time TEC for different experimental storm onset times. Each panel is for a constant longitude; the colors indicate the TEC difference in latitude and local time. The longitude depicted corresponds to the longitude of 1200 LT at the time of onset of storm conditions.

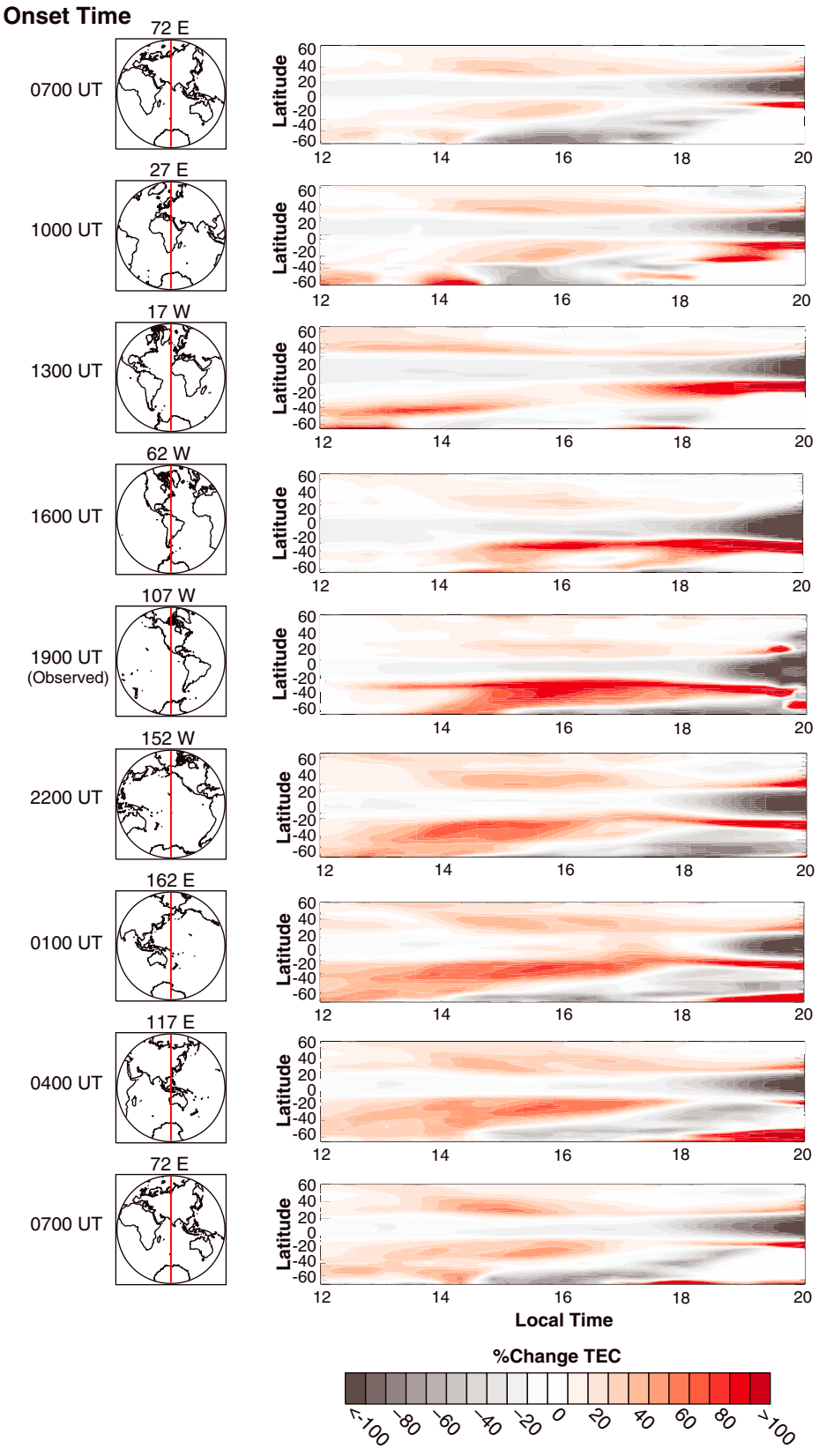

Figure 5. Same as Figure 4 but for the percent change in TEC between quiet conditions and storm conditions.

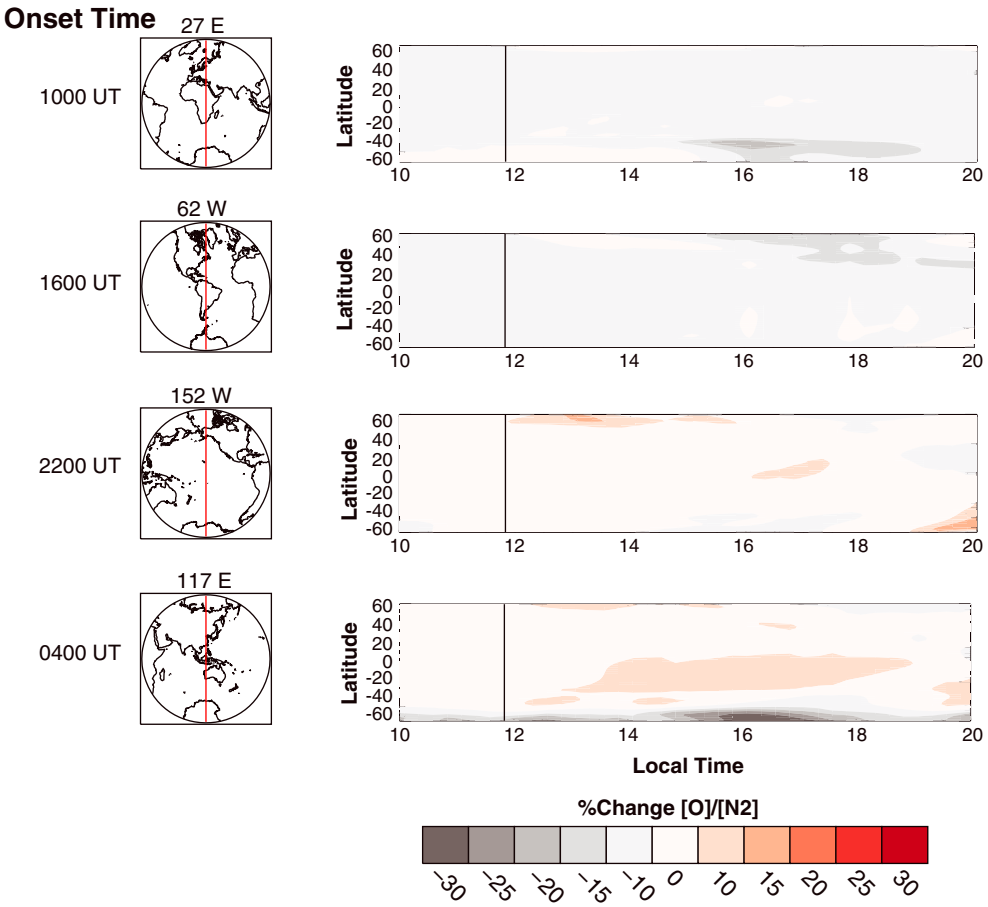

Figure 6. Percent change between quiet and storm time [O]/[N_2] ratio for selected experimental storm onset times. Each panel is for a constant longitude, and the colors indicate the percent change in latitude and local time.

These enhancements develop approximately 2 h after the onset of the storm and extend past sunset. These results indicate that the density and prominence of daytime plasma structures at middle and low latitudes do, in fact, depend on the UT of storm onset (sunward longitude sector) and that GITM is capable of reproducing this effect.

5. Drivers of Variability Impacted by UT Onset

By interrogating the model outputs for each experiment, we can examine drivers of the variability seen in the model by changing the UT (sunward longitude sector) of the storm onset. We consider several drivers including variations in the [O]/[N_2] ratio, neutral winds, and the geomagnetic topology.

5.1. O/N_2 Ratio

Changes in TEC plasma populations, such as those in Figures 4 and 5, may be attributed to changes in the sources or sinks of plasma populations. The [O]/[N_2] ratio is a strong indicator of the population source of plasma in the ionosphere and is a relevant consideration when examining changes in TEC [*Burns et al.*, 1995b]. It is also indicative of the controlling influence of the neutral atmosphere on the ionosphere. Figure 6 shows the percent change in the [O]/[N_2] ratio (storm conditions compared to quiet conditions) for selected experimental runs for constant longitude sectors. In the high latitudes of the Southern Hemisphere, there is a substantial reduction of the [O]/[N_2] ratio of up to 30% near 60° at 1600 LT for storm onsets between 0400 UT and 1000 UT. The reduced [O]/[N_2] ratio likely contributes strongly to the depletion of TEC in this particular geographic area. While the equatorial region indicates a 10–15% decline in [O]/[N_2] ratio (between storm onsets starting at 1000 and 1600 UT) compared to quiet conditions, this is not triggered by the onset of storm conditions and cannot be identified as the main driver of the changes in the plasma populations. Other drivers must be considered.

5.2. Neutral Winds

Given that changes in the loss and production of plasma by way of the [O]/[N_2] ratio do not adequately account for the modeled changes in TEC, an explanation is sought in effects of storm time neutral winds at ionosphere altitudes. Neutral winds drag the embedded plasma along with it. When a component of the neutral wind is parallel to the magnetic field, it can push plasma along the field lines [*Bramley and Young*, 1968; *Burrell et al.*, 2012, 2013]. Enhanced equatorward winds can therefore potentially affect plasma densities by lifting the *F* layer and reducing loss through recombination [*Rishbeth et al.*, 1987]. While the plasma resists moving across magnetic field lines, other factors may induce vertical drift. As the electric field is modified by disturbance winds, storm-driven electric fields may penetrate to lower latitudes due to an active ring current; phenomena such as subauroral polarization stream (SAPS) and disturbance dynamo-driven currents prompt potentials that can cause the plasma to drift upward as well [*Blanc and Richmond*, 1980; *Heelis*, 2004]. Therefore, both zonal and meridional winds are considered as potential sources of TEC disturbance, and the potential UT dependence of these drivers is investigated.

Wind vectors for the experimental model runs at 307 km are shown in Figure 7. Each panel is for a constant longitude; the contoured colors behind the vectors indicate the change in the zonal wind from quiet conditions in latitude and local time.

At local noon and storm onset, *F* region winds are generally westward at low latitudes in all experiments. However, onsets between 0400 and 1000 UT show moderate winds that are more Eastward in the middle- and high-latitude Southern Hemisphere at noon. Two hours later, the wind vectors at 1400 LT show strikingly different behaviors between the different experiments, where both the magnitudes and directions of the winds are variable between longitudes. There is a strong band of eastward winds near 45°S which persists throughout in all experiments, except those with onset times of 1600 UT and 1900 UT. In sectors expected to be near the auroral oval in the Southern Hemisphere, there is a pronounced acceleration of winds.

Zonal wind differences between quiet and storm time are on the order of 100–200 m/s throughout low and middle latitudes, growing as the storm continues in the 8 h following onset shown in Figure 7. The zonal winds in the equatorial region become more eastward (antisunward) through the rest of the afternoon compared to quiet conditions. Though the simulation predicts large changes in *F* region winds, variations in the zonal winds are not consistent with being the main driver of the TEC changes shown earlier. The meridional effects are much smaller and not of the magnitude necessary to produce a major uplift of the *F* layer that might influence the balance of *F* layer production and loss.

While there is significant variation between longitudes in the neutral winds, the impact of these winds on the plasma distribution is intimately coupled to the geomagnetic topology as the charged particles are constrained by the magnetic field lines. Given that Earth's geomagnetic field is tilted, any $E \times B$ drift will therefore have a vertical component [*Deng and Ridley*, 2006]. The influence of the neutral wind needs to be considered in combination with Earth's geomagnetic field in order to understand the 3-D motion of the plasma which may be inducing the TEC structures seen in this experiment.

5.3. Geomagnetic Topology

Plasmas embedded within the neutral winds interact with and are constrained by Earth's nonuniform geomagnetic topology. Previous studies have found that as a disturbance from a solar flare propagates through the nightside and back to the dayside, the magnetic field may have a large impact on the response of the ionosphere [*Zhu and Ridley*, 2014]. The International Geomagnetic Reference Field (IGRF) [*Finlay et al.*, 2010] intensity (10 nT) for August 2011 is shown in Figure 8 as solid black contours. Earth has an irregular quasi-dipole field that is both tilted and offset from the planet's axis of rotation. Large anomalies exist in this field: at the equator, the poles, and particularly around South America [*Knecht and Shuman*, 1985; *Malin and Isakara*, 1976]. Overlaid on the IGRF intensity is vertical plasma velocity at 1600 LT (4 h after the onset of the storm) for the modeling experiments shown in Figure 7. This local time was chosen because it is the local time with the greatest changes between modeling experiments as seen in TEC (Figure 2).

Vertical plasma motion shows extensive variability in latitude, local time (not shown), and between modeling experiments. During quiet conditions there is an equatorial band of rising plasma, while off the equator, plasma is descending as expected along magnetic field lines. Stronger descent is seen over the South Atlantic anomaly. However, during storm conditions, plasma there has less descent at nearly all latitudes with the exception of longitudes around south of Africa. In the final panel, the difference between storm and quiet ion

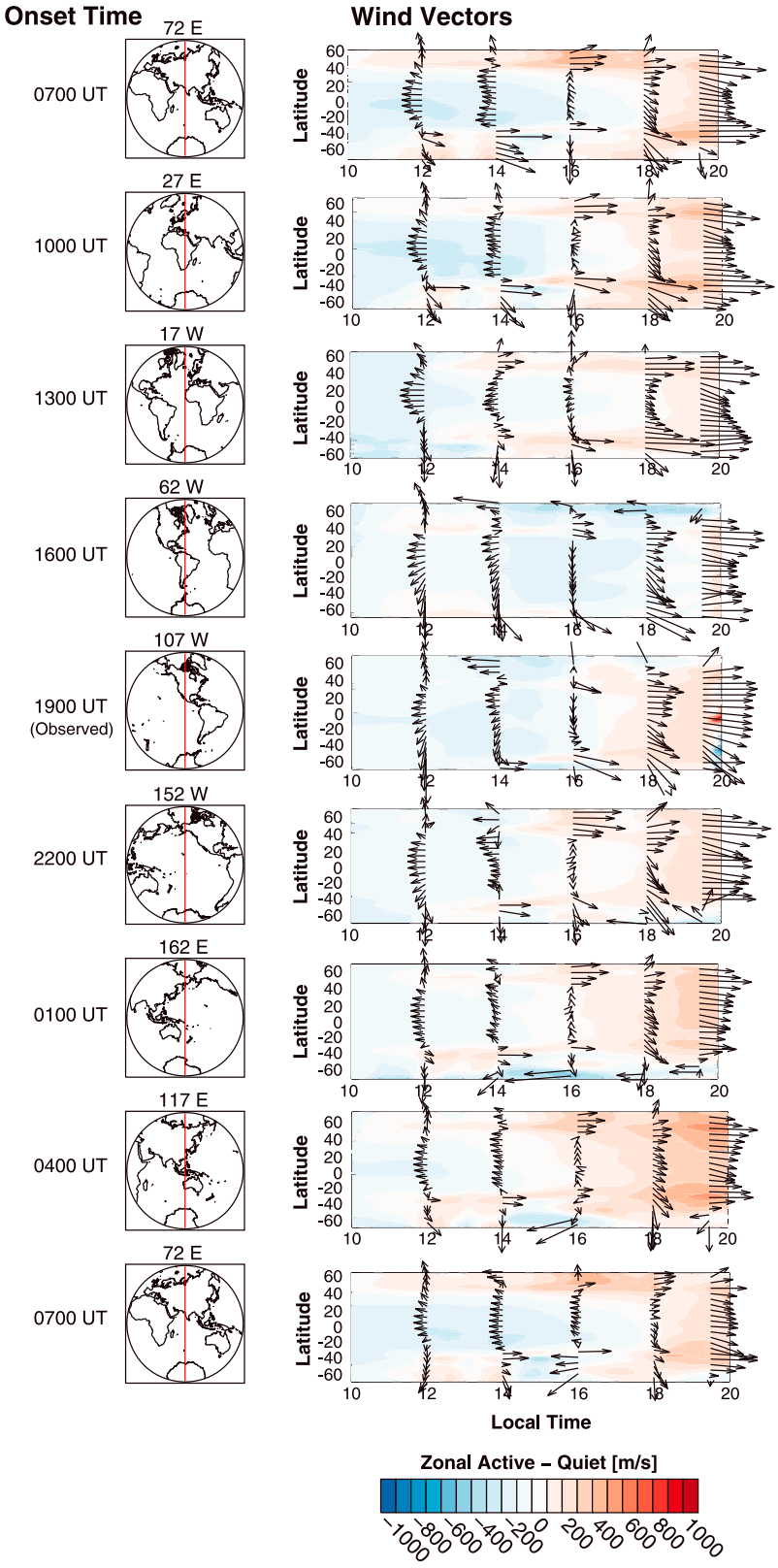

Figure 7. Wind vectors for the experimental storm onset times. Each panel is for a constant longitude; the contoured colors behind the vectors indicate the zonal wind change in latitude and local time. The longitude depicted corresponds to the longitude of 1200 LT at the time of the onset of storm conditions.

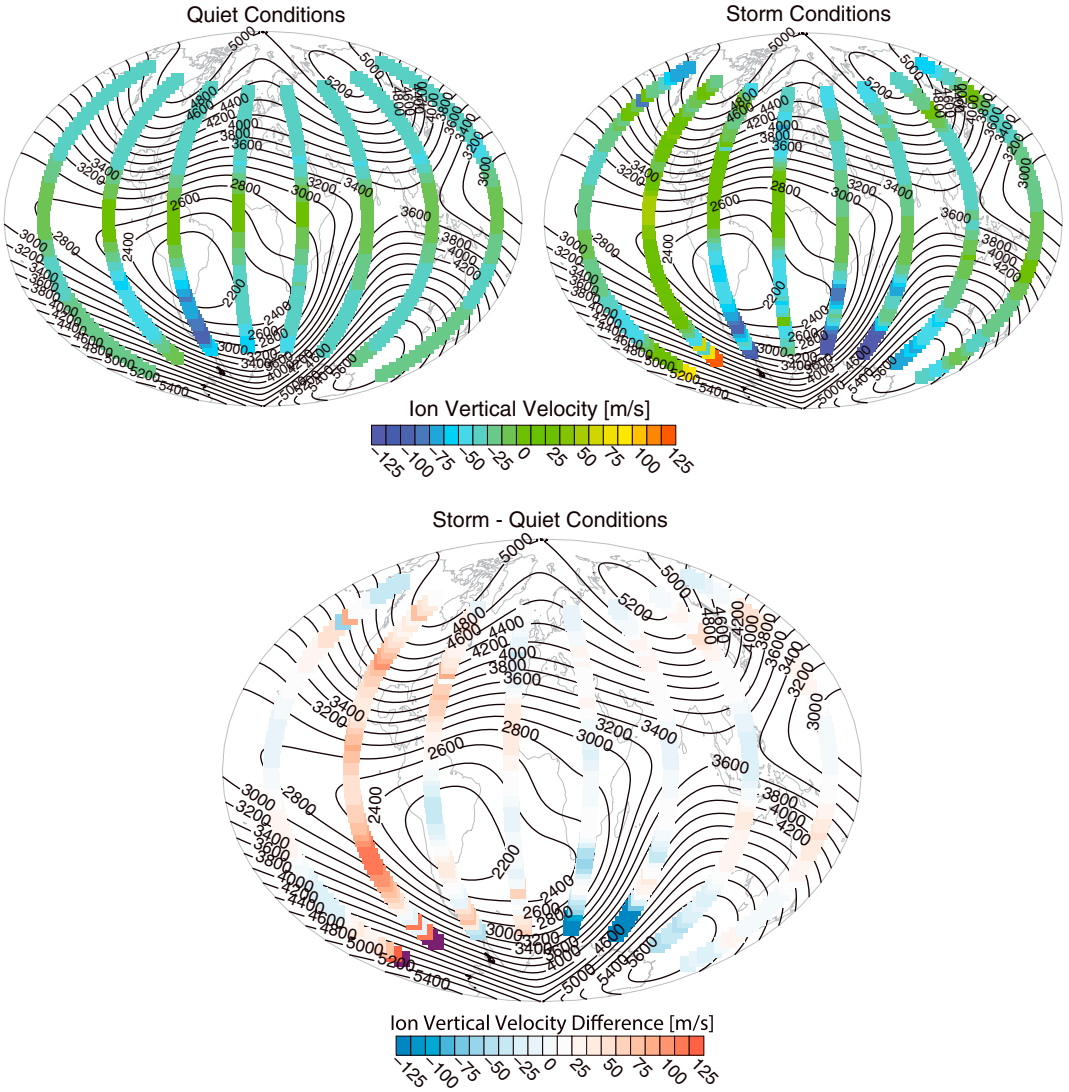

Figure 8. August 2011 International Geomagnetic Reference Field (IGRF) intensity (10 nT) are plotted as solid black contours. The ion vertical velocity (m/s) at 1600 LT for the modeling experiments shown in Figure 7 are shown for quiet conditions, the August 2011 geomagnetic storm conditions, and the difference between these conditions (storm − quiet).

vertical velocities is shown. However, this vertical ion motion varies greatly by longitude sector. There is a zonal band of increased vertical ion motion in the Northern Hemisphere at middle and low latitudes that peaks in over North America. Critically, there is one longitude sector that stands out in particular: the Americas and eastern Pacific longitude sector of the storm that develops at 1900 UT. This sector experiences more vertical motion than any other at nearly all latitudes. As the plasma is lofted higher in altitude it experiences reduced loss (by recombination), which leads to higher TEC. Southern hemispheric preferences may be due not only to seasonal differences but also because of the greater separation between the geographic and geomagnetic poles [*Fuller-Rowell et al.*, 1988]. Given the limited correspondence between the TEC variation and other parameters shown, we conclude that this property is the critical and determining factor in the development of increased low and middle latitude plasma in this sector during storms.

6. Conclusions

We have performed a series of modeling experiments with GITM in which the August 2011 geomagnetic storm solar wind inputs were shifted in universal time, such that different longitude sectors were sunward when the storm commenced. GITM shows a remarkable UT-dependent effect of ionospheric conditions at

low latitudes following storm onset. Specifically, the 1900 UT sector at onset produces the largest enhancement in ionospheric TEC at low to middle latitudes, particularly in the Southern Hemisphere. Further, this result matched the relatively sparse observations of UT variation in storm time ionospheric effects observed in global TEC maps by *Immel and Mannucci* [2013], which showed a similar relationship between the UT onset time of a given storm and the structure and evolution of TEC in the middle-latitude ionosphere, favoring (again) the Southern Hemisphere. In a broader sense, during this modeled geomagnetic storm period, larger TEC were produced by GITM over the American and eastern Pacific longitude sectors of the afternoon Southern Hemisphere, which corresponds to storms that develop between 1600 and 2400 UT. For communications and navigation technologies that have critical dependencies on ionospheric conditions, these results imply larger impacts on their availability for storms that develop between these hours.

Possible driving mechanisms for this longitudinal asymmetry were found to include changes in $[O]/[N_2]$ ratios, changes in the neutral winds, and asymmetries in Earth's geomagnetic topology. In the high-latitude Southern Hemisphere a 30% reduction in the $[O]/[N_2]$ ratio is likely responsible for strong depletions in TEC. However, changes in $[O]/[N_2]$ ratios could not account for the changes and structure of TEC in low and middle latitudes. The neutral horizontal winds at *F* region altitudes showed marked variability between model experiments, but the motion of plasma is also closely coupled to Earth's magnetic field. It is likely that the explanation for the longitudinal and UT dependence of the ionosphere is that it is driven by changes in neutral winds and interaction with Earth's tilted and distorted magnetic field, which reaches its most southern latitudes and greatest gradient in declination in the South American sector.

Acknowledgments

This work was supported by NSF grants AGS1103333 and AGS1019065. GITM was driven from time-shifted inputs archived by the Space Weather Modeling Framework at the Goddard Space Flight Center's Community Coordinated Modeling Center and can be accessed at http://ccmc.gsfc.nasa.gov/ungrouped/GM_IM/GM_main.php by searching for the string "Greer." The link to the ACE data depository is http://www.srl.caltech.edu/ACE/ASC/level2/index.html, and the data are also available at http://cdaweb.gsfc.nasa.gov/. The National Oceanic and Atmospheric Administration (NOAA) provided hemispheric power index data (http://www.swpc.noaa.gov/ftpmenu/lists/hpi.html) to drive the high-latitude auroral precipitation. The results from the GITM simulations are publicly available. Because of the considerable amount of data (several gigabytes), the results can only be obtained on request from the main author. The GITM model was developed by the University of Michigan (contact: Aaron Ridley, ridley@umich.edu). We would like to acknowledge high-performance computing support from Yellowstone provided by NCAR's Computational and Information Systems Laboratory, sponsored by the National Science Foundation.

References

Aarons, J. (1991), The role of the ring current in the generation or inhibition of equatorial *F* layer irregularities during magnetic storms, *Radio Sci.*, *26*(4), 1131–1149, doi:10.1029/91RS00473.

Abdu, M., I. Batista, A. Carrasco, and C. Brum (2005), South Atlantic magnetic anomaly ionization: A review and a new focus on electrodynamic effects in the equatorial ionosphere, *J. Atmos. Sol. Terr. Phys.*, *67*(17-18), 1643–1657, doi:10.1016/j.jastp.2005.01.014.

Blanc, M., and A. D. Richmond (1980), The ionospheric disturbance dynamo, *J. Geophys. Res.*, *85*, 1669–1688.

Bramley, E., and M. Young (1968), Winds and electromagnetic drifts in the equatorial F_2-region, *J. Atmos. Terr. Phys.*, *30*(1), 99–111, doi:10.1016/0021-9169(68)90044-5.

Burch, J. (2003), The first two years of Image, in *Magnetospheric Imaging—The Image Prime Mission*, edited by J. Burch, pp. 1–24, Springer, Netherlands.

Burns, A. G., T. L. Killeen, W. Deng, and G. R. Carignan (1995a), Geomagnetic storm effects in the low- to middle-latitude upper thermosphere, *J. Geophys. Res.*, *100*, 14,673–14,691.

Burns, A. G., T. L. Killeen, G. R. Carignan, and R. G. Roble (1995b), Large enhancements of the O/N_2 ratio in the evening sector of the winter hemisphere during geomagnetic storms, *J. Geophys. Res.*, *100*, 14,673–14,691.

Burrell, A. G., R. A. Heelis, and R. A. Stoneback (2012), Equatorial longitude and local time variations of topside magnetic field-aligned ion drifts at solar minimum, *J. Geophys. Res.*, *117*, A04304, doi:10.1029/2011JA017264.

Burrell, A. G., R. A. Heelis, and A. Ridley (2013), Daytime altitude variations of the equatorial, topside magnetic field-aligned ion transport at solar minimum, *J. Geophys. Res. Space Physics*, *118*, 3568–3575, doi:10.1002/jgra.50284.

Carpenter, D. L., A. J. Smith, B. L. Giles, C. R. Chappell, and P. M. E. Decreau (1992), A case study of plasma structure in the dusk sector associated with enhanced magnetospheric convection, *J. Geophys. Res.*, *97*, 1157–1166.

Coster, A. J., M. J. Colerico, J. C. Foster, W. Rideout, and F. Rich (2007), Longitude sector comparisons of storm enhanced density, *Geophys. Res. Lett.*, *34*, L18105, doi:10.1029/2007GL030682.

Deng, Y., and A. Ridley (2006), The role of vertical ion convection in the high-latitude ionospheric plasma distribution, *J. Geophys. Res.*, *97*, 1157–1166, doi:10.1029/2006JA011637.

Deng, Y., A. D. Richmond, A. J. Ridley, and H.-L. Liu (2008), Assessment of the non-hydrostatic effect on the upper atmosphere using a general circulation model (GCM), *Geophys. Res. Lett.*, *35*, L01104, doi:10.1029/2007GL032182.

England, S. L., S. Maus, T. J. Immel, and S. B. Mende (2006), Longitudinal variation of the *E*-region electric fields caused by atmospheric tides, *Geophys. Res. Lett.*, *33*, L21105, doi:10.1029/2006GL027465.

Fejer, B. G., L. Scherliess, and E. R. de Paula (1999), Effects of the vertical plasma drift velocity on the generation and evolution of equatorial spread *F*, *J. Geophys. Res.*, *104*, 19,859–19,870, doi:10.1029/1999JA900271.

Finlay, C. C., et al. (2010), International geomagnetic reference field: The eleventh generation, *Geophys. J. Int.*, *183*(3), 1216–1230, doi:10.1111/j.1365-246X.2010.04804.x.

Forbes, J. M., X. Zhang, S. Palo, J. Russell, C. J. Mertens, and M. Mlynczak (2008), Tidal variability in the ionospheric dynamo region, *J. Geophys. Res.*, *113*, A02310, doi:10.1029/2007JA012737.

Foster, J. C., and F. J. Rich (1998), Prompt mid-latitude electric field effects during severe geomagnetic storms, *J. Geophys. Res.*, *103*, 26,367–26,372, doi:10.1029/2007JA012737.

Fuller-Rowell, T., D. Rees, S. Quegan, R. Moffett, and G. Bailey (1988), Simulations of the seasonal and universal time variations of the high-latitude thermosphere and ionosphere using a coupled, three-dimensional, model, in *Ionospheric Modelling*, edited by T. Fuller-Rowell et al., pp. 189–217, Birkhäuser, Basel, Switzerland.

Fuller-Rowell, T. J., M. V. Codrescu, R. J. Moffett, and S. Quegan (1994), Response of the thermosphere and ionosphere to geomagnetic storms, *J. Geophys. Res.*, *99*, 3893–3914.

Grebowsky, J. M., I. Hoffman, and N. C. Maynard (1978), Ionospheric and magnetospheric "plasmapauses", *Planet. Space Sci.*, *26*(7), 651–660, doi:10.1016/0032-0633(78)90098-3.

Hajj, G., and L. Romans (1998), Ionospheric electron density profiles obtained with the Global Positioning System: Results from the GPS/MET experiment, *Radio Sci.*, *33*(1), 175–190, doi:10.1029/97RS03183.

Hedin, A. E. (1987), MSIS-86 thermospheric model, *J. Geophys. Res.*, *92*(11), 4649–4662.
Heelis, R. A. (2004), Electrodynamics in the low and middle latitude ionosphere: A tutorial, *J. Atmos. Terr. Phys.*, *66*, 825–838, doi:10.1016/j.jastp.2004.01.034.
Ho, C. M., A. J. Mannucci, U. J. Lindqwister, X. Pi, and B. T. Tsurutani (1996), Global ionosphere perturbations monitored by the worldwide GPS network, *Geophys. Res. Lett.*, *23*(22), 3219–3222, doi:10.1029/96GL02763.
Huang, C.-S., J. C. Foster, and M. C. Kelley (2005), Long-duration penetration of the interplanetary electric field to the low-latitude ionosphere during the main phase of magnetic storms, *J. Geophys. Res.*, *110*, A11309, doi:10.1029/2005JA011202.
Huang, C. Y., Y.-J. Su, E. K. Sutton, D. R. Weimer, and R. L. Davidson (2014), Energy coupling during the August 2011 magnetic storm, *J. Geophys. Res. Space Physics*, *119*, 1219–1232, doi:10.1002/2013JA019297.
Immel, T. J., and A. J. Mannucci (2013), Ionospheric redistribution during geomagnetic storms, *J. Geophys. Res. Space Physics*, *118*, 7928–7939, doi:10.1002/2013JA018919.
Immel, T. J., E. Sagawa, S. L. England, S. B. Henderson, M. E. Hagan, S. B. Mende, H. U. Frey, C. M. Swenson, and L. J. Paxton (2006), Control of equatorial ionospheric morphology by atmospheric tides, *Geophys. Res. Lett.*, *33*, L15108, doi:10.1029/2006GL026161.
Jakowski, N., S. Heise, A. Wehrenpfennig, S. Schlüter, and R. Reimer (2002a), GPS/GLONASS based TEC measurements as contributor for space weather forecast, *J. Atmos. Sol. Terr. Phys.*, *64*(5–6), 729–735, doi:10.1016/S1364-6826(02)00034-2.
Jakowski, N., A. Wehrenpfennig, S. Heise, C. Reigber, H. Lühr, L. Grunwaldt, and T. K. Meehan (2002b), GPS radio occultation measurements of the ionosphere from CHAMP: Early results, *Geophys. Res. Lett.*, *29*(10), 1457, doi:10.1029/2001GL014364.
Kelley, M. C., M. N. Vlasov, J. C. Foster, and A. J. Coster (2004), A quantitative explanation for the phenomenon known as storm-enhanced density, *Geophys. Res. Lett.*, *31*, L19809, doi:10.1029/2004GL020875.
Kintner, P. M., and B. M. Ledvina (2005), The ionosphere, radio navigation, and global navigation satellite systems, *Adv. Space Res.*, *35*(5), 788–811, doi:10.1016/j.asr.2004.12.076.
Klimenko, V., and M. Klimenko (2015), EEJ and EIA variations during modeling substorms with different onset moments, *Adv. Space Res.*, *56*(9), 1982–1991, doi:10.1016/j.asr.2015.07.041.
Knecht, D. J., and B. M. Shuman (1985), The geomagnetic field, in *Handbook of Geophysics and the Space Environment*, edited by D. J. Knecht and and B. M. Shuman, 4 p., Air Force Geophys. Lab., Springfield, Va.
Komjathy, A., L. Sparks, A. J. Mannucci, and A. Coster (2005), The ionospheric impact of the October 2003 storm event on wide area augmentation system, *GPS Solut.*, *9*(1), 41–50, doi:10.1007/s10291-004-0126-2.
Kouba, J. (2009), A Guide to Using International GNSS Service (IGS) Products, International GNSS Service, Ottawa. [Available at http: //igscb.jpl.nasa.gov/igscb/resource/pubs/UsingIGSProductsVer21.pdf.]
Lei, J., et al. (2007), Comparison of cosmic ionospheric measurements with ground-based observations and model predictions: Preliminary results, *J. Geophys. Res.*, *112*, A07308, doi:10.1029/2006JA012240.
Malin, S., and A. M. Isakara (1976), Annual variation of the geomagnetic field, *Geophys. J. R. Astron. Soc.*, *47*, 445–457.
Mannucci, A. J., B. T. Tsurutani, B. A. Iijima, A. Komjathy, A. Saito, W. D. Gonzalez, F. L. Guarnieri, J. U. Kozyra, and R. Skoug (2005), Dayside global ionospheric response to the major interplanetary events of October 29–30, 2003 "Halloween Storms", *Geophys. Res. Lett.*, *32*, L12S02, doi:10.1029/2004GL021467.
Maute, A., M. E. Hagan, V. Yudin, H.-L. Liu, and E. Yizengaw (2015), Causes of the longitudinal differences in the equatorial vertical $E \times B$ drift during the 2013 SSW period as simulated by the TIME-GCM, *J. Geophys. Res. Space Physics*, *120*, 5117–5136, doi:10.1002/2015JA021126.
Mendillo, M. (2006), Storms in the ionosphere: Patterns and processes for total electron content, *Rev. Geophys.*, *44*, RG4001, doi:10.1029/2005RG000193.
Mendillo, M., M. Papagiannis, and J. A. Klobuchar (1970), Ionospheric storms at mid-latitudes, *Radio Sci.*, *5*, 895–898, doi:10.1029/RS005i006p00895.
Oladipo, O. A., J. O. Adeniyi, A. O. Olawepo, and P. H. Doherty (2014), Large-scale ionospheric irregularities occurrence at Ilorin, Nigeria, *Space Weather*, *12*, 300–305, doi:10.1002/2013SW000991.
Pawlowski, D. J., and A. J. Ridley (2009), Quantifying the effect of thermospheric parameterization in a global model, *J. Atmos. Sol. Terr. Phys.*, *71*(1718), 2017–2026, doi:10.1016/j.jastp.2009.09.007.
Pawlowski, D. J., A. J. Ridley, I. Kim, and D. S. Bernstein (2008), Global model comparison with Millstone Hill during September 2005, *J. Geophys. Res.*, *113*, A01312, doi:10.1029/2007JA012390.
Phani Chandrasekhar, N., K. Arora, and N. Nagarajan (2014), Characterization of seasonal and longitudinal variability of EEJ in the Indian region, *J. Geophys. Res. Space Physics*, *119*, 10,242–10,259, doi:10.1002/2014JA020183.
Richmond, A. D. (1995), Ionospheric electrodynamics using magnetic APEX coordinates, *J. Geomagn. Geoelectr.*, *47*(2), 191–212, doi:10.5636/jgg.47.191.
Ridley, A. J., Y. Deng, and G. Tóth (2006), The global ionosphere thermosphere model, *J. Atmos. Sol. Terr. Phys.*, *68*, 839–864, doi:10.1016/j.jastp.2006.01.008.
Rishbeth, H., T. J. Fuller-Rowell, and D. Rees (1987), Diffusive equilibrium and vertical motion in the thermosphere during a severe magnetic storm: A computational study, *Planet. Space Sci.*, *35*, 1157–1165, doi:10.1016/0032-0633(87)90022-5.
Sandel, B. R., R. A. King, W. T. Forrester, D. L. Gallagher, A. L. Broadfoot, and C. C. Curtis (2001), Initial results from the IMAGE Extreme Ultraviolet imager, *Geophys. Res. Lett.*, *28*(8), 1439–1442, doi:10.1029/2001GL012885.
Sojka, J. J., M. David, R. W. Schunk, and R. A. Heelis (2012), A modeling study of the longitudinal dependence of storm time mid-latitude dayside total electron content enhancements, *J. Geophys. Res.*, *117*, A02315, doi:10.1029/2011JA017000.
Sugiura, M. (1964), Hourly values of equatorial *Dst* for the IGY, in *Annual International Geophysical Year*, vol. 35, 9 p., Pergamon, New York.
Tóth, G., et al. (2005), Space Weather Modeling Framework: A new tool for the space science community, *J. Geophys. Res.*, *110*, A12226, doi:10.1029/2005JA011126.
Valladares, C. E., and J. L. Chau (2012), The Low-latitude Ionosphere Sensor network: Initial results, *Radio Sci.*, *47*, RS0L17, doi:10.1029/2011RS004978.
Vichare, G., A. Ridley, and E. Yiğit (2012), Quiet-time low latitude ionospheric electrodynamics in the non-hydrostatic Global Ionosphere–Thermosphere Model, *J. Atmos. Sol. Terr. Phys.*, *80*, 161–172.
Weimer, D. R. (1996), A flexible, IMF dependent model of high-latitude electric potentials having "space weather" applications, *Geophys. Res. Lett.*, *23*, 2549–2552, doi:10.1029/96GL02255.
Yizengaw, E., M. B. Moldwin, E. Zesta, C. M. Biouele, B. Damtie, A. Mebrahtu, B. Rabiu, C. F. Valladares, and R. Stoneback (2014), The longitudinal variability of equatorial electrojet and vertical drift velocity in the African and American sectors, *Ann. Geophys.*, *32*(3), 231–238, doi:10.5194/angeo-32-231-2014.

Zhu, J., and A. J. Ridley (2014), The effect of background conditions on the ionospheric response to solar flares, *J. Geophys. Res. Space Physics*, *119*, 5060–5075, doi:10.1002/2014JA019887.

Zhu, J., and A. J. Ridley (2016), Investigating the performance of simplified neutral-ion collisional heating rate in a global IT model, *J. Geophys. Res. Space Physics*, *121*, 578–588, doi:10.1002/2015JA021637.

Zhu, J., A. J. Ridley, and Y. Deng (2016), Simulating electron and ion temperature in a global ionosphere thermosphere model: Validation and modeling an idealized substorm, *J. Atmos. Sol. Terr. Phys.*, *138-139*, 243–260, doi:10.1016/j.jastp.2016.01.005.